Spontaneous parity-breaking transition in directional growth of lamellar eutectic structures

K. Kassner
Institut für Festkörperforschung des Forschungszentrums Jülich, 517 Jülich, Germany

C. Misbah
Groupe de Physique des Solides, Université Paris VII et Paris VI, Place Jussieu, 75005 Paris, France
(Received 25 April 1991; revised manuscript received 18 July 1991)

A full study of parity-broken states in the directional solidification of lamellar eutectics is performed within the boundary-integral formulation. Symmetric states cease to exist at a wavelength λ, which is approximately twice that corresponding to their minimum undercooling, whereas solutions with a broken parity, drifting transversely to the growth front, appear as a forward bifurcation. Our results suggest that if one effectively doubles the wavelength of the initially symmetric state—a situation that can be achieved via a sudden jump of the velocity V by a factor of about 4, since $\lambda^2 V \simeq$const—then tilted lamellae should appear as extended states and not as "solitons." We find here that parity-broken states exist for hypereutectic as well as for hypoeutectic and eutectic compositions. We have extended the derivation of the similarity equation derived previously [K. Kassner and C. Misbah, Phys. Rev. Lett. **66**, 445 (1991)] to the present situation. This case involves additional subtleties, due to the loss of reflection symmetry about the growth axis. Among other results, we find that the tilt angle ϕ should depend on $\sigma = d_0 l/\lambda^2$ and $\chi = l/l_T$ only, where d_0, l, and l_T are the capillary, diffusion, and thermal lengths, respectively, and λ is the wavelength of the pattern. At large enough growth velocities V, $\phi \simeq \phi(\sigma)$, while at small V the dependence on χ is strong. These predictions can be tested experimentally.

PACS number(s): 61.50.Cj, 05.70.Fh, 81.30.Fb, 68.70.+w

I. INTRODUCTION

When eutectics grow by directional solidification as thin films, they generally form a parallel array of the two coexisting solid phases [1–3] α and β. Under some conditions a few tilted lamellae appear [4]. Such a phenomenon was described by metallurgists at least 20 years ago [5]. It was often attributed to the locking on strong crystalline anisotropies. Only after the discovery by Simon, Bechhofer, and Libchaber [6] of a similar phenomenon during the growth of a nematic crystal from its isotropic phase have these parity-broken states gained renewed interest. In that system, localized inclusions of asymmetric cells appear that drift transversely to the growth front. Another system where parity-broken cells were observed is the viscous fingering one of Rabaud, Michalland, and Couder [7]. Faivre *et al.* [4] have focused on tilted growth of lamellar eutectics, in which we are interested here. An outcome of their experimental investigation was that after a small jump of the growth velocity a few tilted lamellae appear, drifting sideways at constant velocity.

The fact that the appearance of domains of asymmetric cells is common to systems that look diverse could indicate that this phenomenon may be simply a disguised form of only few prototypes. An important step was made by Coullet, Goldstein, and Gunaratne [8] who suggested that these travelling modes are localized inclusions of a new asymmetric state, which may result from a bifurcation of the underlying symmetric one. They have developed a phenomenological model that captures some interesting features seen in the experiments of Simon, Bechhofer, and Libchaber [6]. It remains to be shown, however, whether the microscopic models of growth do support parity-broken states. In this paper we are concerned with the theory of asymmetric lamellar eutectic structures. If one admits the idea of Coullet, Goldstein, and Gunaratne [8], one should expect that there exist—in a certain range of the physical parameters—periodic tilted solutions which extend along the whole front. Tilted growth should then appear as a result of a bifurcation of the symmetric solution. We have recently shown [9] that the fully isotropic model of eutectics supports tilted solutions with a well-defined tilt angle. Here we will devote an extensive study to this phenomenon and make new predictions that are not devoid of experimental testability. Moreover we will generalize the derivation of the so-called similarity equation [10,11] to the present case. Let us be more specific by summarizing the main lines that are treated in this paper and their far-reaching consequences.

(i) The boundary-integral equation that governs one-dimensional deformations is solved numerically to search for extended tilted solutions. This is a nonlinear eigenvalue problem for the tilt angle ϕ. It is found that parity-broken states appear as a forward bifurcation of the basic symmetric solutions. We will, up to that point, largely repeat, though in an extensive way, our previous results [9]. Here we will discuss the implication of our results in experiments. In particular we suggest that, since the bifurcation is forward, there is a simple—in principle—experimental protocol to have access to a situation where extended domains of tilted lamellae appear instead of localized solitary modes. Indeed, as will be

seen here, an important result of our analysis is that the asymmetric state appears, for a fixed wavelength λ, at a critical velocity V_c that provides a wavelength $\lambda_{\min}$ for the untilted state with the minimum undercooling, which is approximately half the value of λ: $\lambda_{\min} \simeq \lambda/2$. As a consequence, if one imposes on the symmetric state a wavelength that is (approximately) twice as large as the one it naturally *selects,* it should lose its stability. Since $\lambda_{\min} \sim V^{-1/2}$, and since phase diffusion seems to be a very slow process, a sudden velocity jump by a factor of about 4 should accomplish the required situation. If the experimental sample is homogeneous enough, we expect the tilted state to appear everywhere. This is one of the important consequences of our findings.

(ii) We find that parity-broken states exist for hypereutectic, as well as for eutectic and hypoeutectic compositions. There has been so far, to our knowledge, no experimental evidence reported for the latter two cases. Moreover, in an interesting paper Karma [12], using a random walk model, found a tilting instability for off-eutectic compositions only. If we believe that the tilting instability bears on parity-breaking bifurcations, our results are to be contrasted to those following from the random-walk model of Karma [12].

(iii) We give another useful picture of the pattern formation. Indeed we compute the average front undercooling as a function of λ for both symmetric and asymmetric states. The axisymmetric growth has been extensively described in a recent work [11]. For axisymmetric solutions there is a foldlike mechanism whereby solutions with a wavelength $\lambda \simeq 2\lambda_{\min}$ cease to exist and then merge with parity-broken states. Slightly above the fold singularity the average undercooling (for tilted solution) takes on a minimum. We suspect that the selected asymmetric state operates, as seems to do the symmetric one, at that minimum. This criterion, if it is valid, should provide the wavelength and the tilt angle of the pattern.

(iv) We shall devote some of this work to similarity considerations. We have extended the derivation of the similarity equation [10] to the present case. Some additional subtleties arise. We shall, however, avoid here going through the derivation and refer the reader to another work [13] where an extensive treatment has been presented.

The scheme of this paper is as follows. In Sec. II we provide the basic equations for lamellar eutectic growth and convert them into a closed integrodifferential equation for the front profile. We then briefly describe the numerical strategy to solve the boundary integral equation. Section III is devoted to the results. Section IV contains a rather short discussion of the similarity equation and some of its consequences. Section V discusses some aspects of the results and their implications. In Sec. VI we summarize the results. Some technical details are relegated to the Appendix.

II. BASIC EQUATIONS

The basic equations that govern the front dynamics and the main assumptions that are used have been presented in a recent paper [11] hereafter referred to as I.

Let $u=(c-c_e)/\Delta c$ denote the dimensionless concentration field, where c_e is the equilibrium eutectic concentration (Fig. 1) and $\Delta c = c_\beta - c_\alpha$, where c_α and c_β are the concentrations of the α and β phases, respectively, at the eutectic temperature. Mass conservation in the liquid phase (diffusion in the solid is ignored) implies

$$\frac{1}{D}\frac{\partial u}{\partial t} = \nabla^2 u + \frac{2}{l}\frac{\partial u}{\partial z} , \tag{2.1}$$

where $l = 2D/V$ (D is the diffusion constant and V the pulling speed) is the diffusion length. The concentration far ahead of the solidification front is maintained at a constant value c_∞ so that the condition on u reads

$$u(z \to \infty) = \frac{c_\infty - c_e}{\Delta c} \equiv u_\infty . \tag{2.2}$$

u_∞ may be positive (hypereutectic), negative (hypoeutectic), or zero (eutectic). At the liquid-solid interface $[z=\zeta(x,t)]$ mass balance across the liquid-α and liquid-β phase boundaries takes the form:

$$-D\frac{\partial u}{\partial n} = \begin{cases} [(1-k_\alpha)u + \delta]v_n, & \alpha \text{ phase} \\ [(1-k_\beta)u + \delta - 1]v_n, & \beta \text{ phase} , \end{cases} \tag{2.3}$$

where $\delta = (c_e - c_\alpha)/\Delta c$ is the reduced miscibility gap of the α phase and $1-\delta$ that of the β phase. $v_n = (2D/l + \dot{\zeta})n_z$ is the normal velocity of the interface; the normal vector points from the solid into the liquid [14]. k_i ($i=\alpha,\beta$) is the partition coefficient for the coexistence of the solid i and the liquid phase.

For a molecularly rough liquid-solid interface it is legitimate to assume local chemical equilibrium. This results in the Gibbs-Thomson condition at the two boundaries

$$u = \begin{cases} -\zeta/l_T^\alpha - d_0^\alpha \kappa, & \alpha \text{ phase} \\ \zeta/l_T^\beta + d_0^\beta \kappa, & \beta \text{ phase} , \end{cases} \tag{2.4}$$

where

$$l_T^i = \frac{m_i \Delta c}{G}, \quad d_0^i = \frac{\gamma_{il} T_e}{L_i m_i \Delta c} \tag{2.5}$$

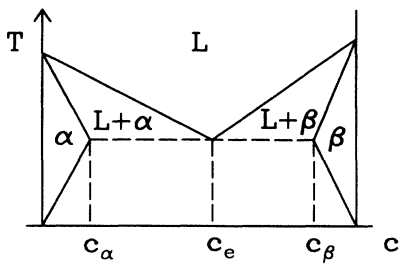

FIG. 1. Generic phase diagram of eutectics. T is the temperature, c the concentration of one component. The regions L, α, and β correspond to one-phase equilibrium states of the liquid, the solid-α, and the solid-β phases, respectively. $L+\alpha$ and $L+\beta$ are regions of two-phase equilibrium between the liquid and one solid phase. c_e, c_α, and c_β denote the equilibrium concentrations of the liquid and the two solid phases at the triple or eutectic point.

are the thermal and capillary lengths, respectively. m_i is the absolute value of the slope of the liquidus line describing coexistence between the liquid and the solid i, G is the applied thermal gradient, γ_{il} is the liquid-solid i interface tension, and L_i is the latent heat per unit volume [16].

Finally local equilibrium applied at the triple point, where the three phases intersect, imposes

$$\gamma_{\alpha\beta}+\gamma_{\alpha L}+\gamma_{\beta L}=0 , \tag{2.6}$$

where γ_{ij} designates the surface tension between phase i and phase j, which is here taken to be isotropic. If the magnitudes of the surface tensions are known, then Eq. (2.6) determines uniquely the contact angles for axisymmetric lamellae (see Fig. 2). Let θ_α and θ_β denote these two angles. For a tilted pattern with a tilt angle ϕ, the angles between the tangents at the liquid-α, β intersections and the horizontal axis (see Fig. 2) at the two ends of a given lamella are different (because of asymmetry.) Let $\tilde{\theta}_\alpha, \tilde{\theta}'_\alpha$ and $\tilde{\theta}_\beta, \tilde{\theta}'_\beta$ denote these two angles for the α and β phase, respectively. Figure 2 shows the pinning angles at the liquid-α, β, and the solid-solid line intersection. It is easy to see from that figure that the pinning angles are related to the contact angles $\theta_{\alpha,\beta}$ by

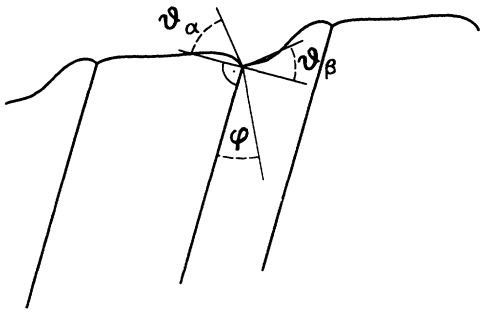

FIG. 2. Illustration of the tilted pattern and the definition of the contact angles.

$$\begin{aligned}&\tilde{\theta}_\alpha=\theta_\alpha-\phi, \quad \tilde{\theta}'_\alpha=\theta_\alpha+\phi ,\\ &\tilde{\theta}_\beta=\theta_\beta+\phi, \quad \tilde{\theta}'_\beta=\theta_\beta-\phi .\end{aligned} \tag{2.7}$$

Note that if the pattern is untilted ($\phi=0$) two of these four conditions become redundant. The set of equations (2.1)–(2.7) completely describes the dynamics of solidification.

The one-sided model we are considering here allows, via Green's functions, to convert the basic equations into a closed nonlinear integrodifferential equation for the front profile [17] $\zeta(x,t)$

$$\begin{aligned}\frac{\omega(\mathbf{r})t}{2}=&\int_{-\infty}^{t-}dt'\int_{-\infty}^{\infty}dx' n_{z'}^{-1}\left[\omega(\mathbf{r}',t')\frac{\partial G}{\partial n'}-G(\mathbf{r},t;\mathbf{r}',t')\frac{\partial\omega(\mathbf{r}',t')}{\partial n'}\right]\\ &-\int_{-\infty}^{t-}dt'\int_{-\infty}^{\infty}dx'[2+\dot{\zeta}(x',t')]G(\mathbf{r},t;\mathbf{r}',t')\omega(\mathbf{r}',t') ,\end{aligned} \tag{2.8}$$

where $\omega\equiv u-u_\infty$, $\mathbf{r}=(x,\zeta(x,t))$, $\mathbf{r}'=(x',\zeta(x',t'))$, and G, the Green function, is given by [17]

$$G(\mathbf{r},t;\mathbf{r}',t')=\frac{\Theta(\Delta t)}{4\pi\Delta t}\exp-\{[\Delta x^2+(\Delta\zeta+2\Delta t)^2]/4\Delta t\} . \tag{2.9}$$

We have introduced the abbreviations $\Delta\zeta=\zeta-\zeta'$, $\Delta x=x-x'$, and $\Delta t=t-t'$ and Θ denotes the Heaviside step function. In Eq. (2.8) lengths and time are reduced by l and l^2/D, respectively.

We are interested in tilted lamellae filling the whole space. Parity-breaking results in a drift of the pattern transversely to the growth front with a drift velocity given by

$$v_d=2\tan(\phi) \tag{2.10}$$

measured in the same units as used in the integral equation (2.8). This means that the front profile

$$\zeta(x,t)=\zeta[x-2t\tan(\phi)] . \tag{2.11}$$

From now on all the x coordinates are understood to be measured in the rest frame of the pattern (that is in the frame moving with v_d in the positive x direction with respect to the laboratory frame). Equation (2.8) can be converted into a stationary equation. It is understood that in order to achieve this we must make the substitution $x\rightarrow x\rightarrow 2t\tan(\phi)$ in the integral equation (2.8). Once this is done we can explicitly integrate over t in Eq. (2.8). The calculation is straightforward. The result can be written in a compact form as

$$\int_{\Gamma_{sl}}d\Gamma' g(\mathbf{r},\mathbf{r}')\frac{\partial\omega(\mathbf{r}')}{\partial n'}=\int_{\Gamma_{sl}}d\Gamma'\omega(\mathbf{r}')h(\mathbf{r},\mathbf{r}') , \tag{2.12}$$

where the integration is performed along the liquid-solid-α + liquid-solid-β boundaries; the whole boundary is denoted by Γ_{sl} (Γ' designates the curvilinear coordinate). g is the stationary propagator and is given by

$$g(\mathbf{r},\mathbf{r}')=\frac{1}{2\pi}e^{-[\Delta\zeta+\Delta x\tan(\phi)]}K_0\left[\frac{\rho}{\cos(\phi)}\right] \tag{2.13}$$

and

$$h(\mathbf{r},\mathbf{r}')=\frac{\partial g(\mathbf{r},\mathbf{r}')}{\partial n'}-2[n_{z'}+n_{x'}\tan(\phi)]g(\mathbf{r},\mathbf{r}')-\tfrac{1}{2}\delta(\mathbf{r}-\mathbf{r}'), \tag{2.14}$$

where $\rho=\sqrt{(\Delta\zeta^2+\Delta x^2)}$, and K_0 is the modified Bessel

function of order zero.

Equation (2.12) together with the four mechanical equilibrium conditions (2.7) completely describe the front morphology of lamellar eutectics. Before describing the numerical strategy to solve the boundary integral equation, we would like first to make some remarks. First note that Eq. (2.12) is a nonlinear eigenvalue problem (of Barenblat-Zeldovich type) for the tilt angle ϕ. This quantity is well defined; it belongs, generically, to a discrete set as can easily be seen from a simple counting argument. Let us consider periodic solutions with periodicity λ. Let $N=N_\alpha+N_\beta$ denote the total number of grid points (Fig. 3) over one period, N_α, N_β being the discretization points on the liquid-α and liquid-β boundary, respectively. Below we will use an intrinsic representation of the interface à la Maclean and Saffman [18], namely we use the angle $\theta(s)$ between the growth axis and normal to the interface, instead of Cartesian coordinates (Fig. 3). We then have $(N_\alpha-1)+(N_\beta-1)$ angle variables. Because the (mean) front position and the volume fraction of the two solid phases are not arbitrary, the origin to fix the front position is also an unknown quantity. Let us take the coordinates of one of the triple points, (ζ_e,x_e) (Fig. 3), to be that origin. We, therefore, have N variables in total. We have in turn N equations. Indeed, we impose the integral equation (2.12) everywhere except at the four points where the three phases intersect. This means that we have $N-4$ equations. At the triple points we require mechanical equilibrium [Eq. (2.7)] instead. The total number of equations is N also. So it seems as if the present problem could be solved for arbitrary values of the tilt angle, since we have, hitherto, made no assumption on that angle. This is, fortunately, not the case. Indeed giving the above N unknowns ($N-2$ angles + ζ_e and x_e) that solve the integral equation (2.12), subject to the mechanical conditions, will not imply, unless accidentally, that the two ends (ζ_1,ζ_N—see Fig. 3) of the integration contour will be at the same height. Hence the condition that our solutions be physical is satisfied by requiring

$$\zeta_1(\phi)-\zeta_N(\phi)=0\ . \tag{2.15}$$

This is a quantization condition that generically leads to the selection of a discrete set of ϕ values.

The numerical method to solve the steady version of the boundary integral equation for symmetric lamellar growth has been extensively described in I. We will, therefore, not repeat here the method. Let us recall that the discretization of the integral equation results (I) into a set of nonlinear algebraic equations. This set of equations obeying the quantization condition (2.15) is solved by means of a Newton-Raphson scheme. As mentioned above the tilt angle ϕ is a well-defined quantity. The tilt angle ϕ can be thought of as an order parameter for parity-broken states. Our procedure for the search of such states consists of fixing the periodicity λ and starting with an appropriate guess for the profile. This guess includes that of the tilt angle. The Newton-Raphson scheme then solves for the $(N+1)$ unknowns: $\{x_e,\zeta_e,\theta_1,\cdots\theta_{N-2},\phi\}$. However, this does not always lead to the sought after solution. Indeed the untilted solution exists for a wide range of parameters and we could not prevent the Newton-Raphson scheme to converge to that solution, although the initial guess seemed appropriate for tilted states. A robust alternative has often consisted of forcing the tilt angle to a fixed value and introducing the growth velocity as a variable. Once the routine has converged, we can progressively vary the parameters to follow the evolution of the solution in certain desired directions of parameter space.

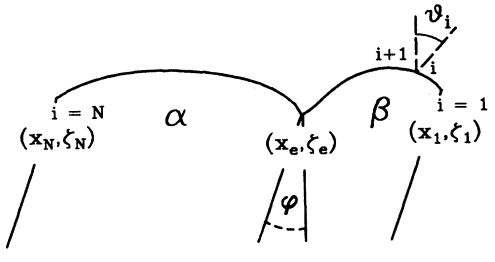

FIG. 3. Discretization elements of the interface. For the discretization procedure and the meaning of the variables see text. Note that the angle belonging to the interval between points i and $i-1$ is θ_i in the β phase and θ_{i-1} in the α phase.

III. THE RESULTS

Let us first define the units in which our results are expressed. In all of this section the units are chosen such that the thermal length $l_T^\alpha=1$ and the diffusion constant $D=1$. In physical units the thermal length is in the range of millimeters and $D\simeq 10^{-5}$ cm^2/s. These values may serve to provide an estimate for the conversion of lengths and velocities, which will be expressed below in the aforementioned units, into physical values. In the figures displaying interface profiles, however, we felt it more appropriate to use the wavelength of the pattern as a length unit. Therefore to make things clear, we will explicitly write x/λ and ζ/λ as a horizontal and vertical symbol in those figures, to be reminded of the used unit.

This section is devoted to the presentation of the main results that emerge from our numerical analysis. For a given wavelength λ we have found a tilted solution that appears at a critical velocity V_c. The physical parameters for the CBr_4-C_2Cl_6 transparent eutectic, used in this calculation, are detailed in the caption of Fig. 4. Figure 4

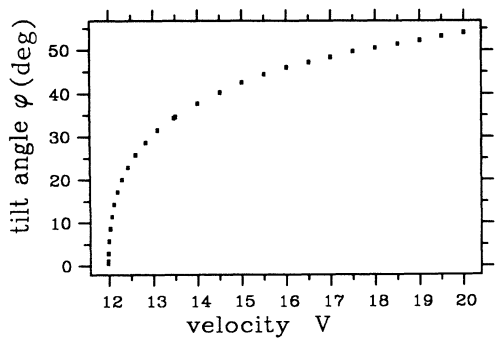

FIG. 4. Bifurcation diagram. The parameters used here are $\lambda=0.012$, $l_T^\alpha=l_T^\beta=1$, $d_0^\alpha=9\times10^{-6}$, $d_0^\beta=5\times10^{-6}$, $k_\alpha=0.99$, $k_\beta=1.04$, $u_\infty=0.05$, $\delta=0.3$, $\theta_\alpha=0.9$, $\theta_\beta=0.7$.

shows the bifurcation diagram. There we represent the tilt angle ϕ as a function of the growth velocity. One sees that the parity-broken state occurs as a result of a forward bifurcation of the symmetric one. The caption of the figure specifies the set of parameters for which Fig. 4 is computed. We should, however, point out that we have computed the same diagram in a wide range of parameters without noticing any qualitative change, in particular the bifurcation remains forward. Shown in Figs. 5 and 6 are the symmetric and asymmetric interface profiles for velocities slightly above the critical one. Note that the tilt angle reaches a finite value even close to V_c. This feature can be traced back to the disparate character of the two competing lengths, namely the diffusion length (of the order of a mm) and the capillary length (of the atomistic scale). This feature of the bifurcation curve is also met in directional solidification of dilute mixtures [19] where the planar front undergoes a Mullins-Sekerka [20] instability, and it expresses the importance of nonlinearities even in the vicinity of the threshold.

It should be noted here that the critical point where the parity-broken state appears corresponds to an instability point of the symmetric state. Indeed this can be understood from a simple symmetry argument in the context of Landau theory, which can always be performed close enough to the critical point.

Let us now give another instructive picture of our results. One of the quantities most often referred to in the discussion of lamellar eutectics is the average front undercooling as a function of the wavelength. It is, therefore, natural to represent what is happening in the λ,Δ plane. The physical front undercooling Δ is defined as

$$\Delta = -G\langle\zeta(x)\rangle \ , \tag{3.1}$$

where $\langle\zeta\rangle$ signifies the mean value over one period. Below we will consider $\Delta/G \equiv -\langle\zeta\rangle$ as a measure of the undercooling instead of Δ itself. In an important paper Jackson and Hunt [21] have demonstrated that the average front undercooling takes on a minimum at a wavelength $\lambda_{\min}$ that is of the order of $\sqrt{d_0 l}$, which is the geometric mean of the two competing lengths, the diffusion and capillary lengths. In the Jackson and Hunt theory [21] and all subsequent developments the existence of steady lamellar eutectics could extend to arbitrary large values of λ. Contrarily, we have demonstrated in a recent article [11], by solving the full boundary integral

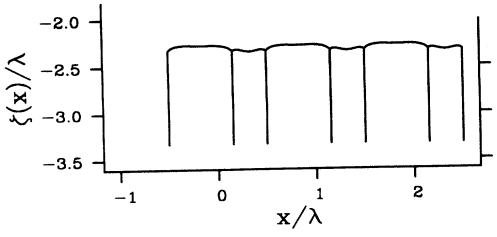

FIG. 5. The symmetric front profile computed close to the critical velocity for the appearance of tilted solutions (see text). $\lambda=0.008$, $d_0^{\alpha}=2\times10^{-5}$; the other parameters are the same as in Fig. 4.

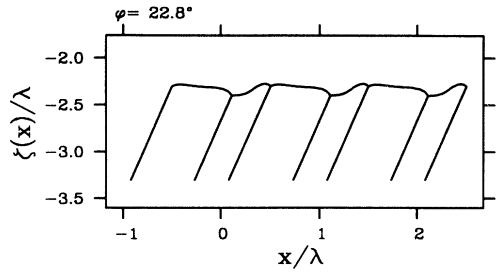

FIG. 6. The asymmetric front profile computed close above the critical velocity (see text). Other parameters as in Fig. 5.

equation, that the symmetric lamellar solutions cease to exist above a wavelength $\lambda \simeq 2\lambda_{\min}$. The solutions run into a fold singularity. We have, moreover, found, for a given λ (below the fold), a discrete set of solutions. Figure 7 shows $-\langle\zeta\rangle$ as a function of λ for both the symmetric and asymmetric solutions. The stars refer to the asymmetric solution while all the other symbols correspond to the symmetric ones. Two remarks are in order. (i) The bifurcation of the asymmetric solution occurs at a value λ slightly below the one where the fold singularity takes place. In other words the symmetric solution becomes unstable before it ceases to exist. (ii) The average undercooling for asymmetric solutions takes on a minimum, too. This minimum is close to the fold. If one uses for the asymmetric state the Cahn argument [22], according to which steady lamellar growth operates at the minimum undercooling, we can predict both the wavelength and the tilt angle ϕ (using the bifurcation diagram). For example, for the set of parameters used here the minimum undercooling for the tilted pattern yields a wavelength $\lambda \simeq 1.9\lambda_{\min}$, $\lambda_{\min}$ being the one providing the minimum undercooling for the symmetric state. If one constructs a bifurcation diagram in the plane (ϕ,λ) (which is basically the same as the one displayed on Fig. 4, for similarity reasons to be discussed in the next section) and uses the value of the wavelength at the

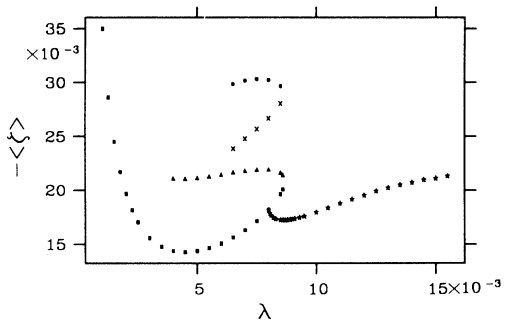

FIG. 7. Average undercooling as a function of λ for four branches of axisymmetric solutions to the model equations (squares, triangles, crosses, and circles) and one branch of tilted solutions. The four branches form two pairs whose members coalesce into a fold singularity at $\lambda \approx 0.0086$. Beyond this λ value, no axisymmetric solutions could be found. The stars correspond to the tilted solution. $V=27.5$, other parameters as in Fig. 5.

minimum undercooling, we obtain $\phi \simeq 23°$. These values seem to be in good agreement with experimental observations. Indeed, the measured ratio of the wavelengths of the asymmetric to the symmetric state is about 2, while the tilt angle $\phi \simeq 25°$.

We should, however, be cautious for the following reasons. First, the physical parameters used here suffer from experimental uncertainties. In particular, an accurate measurement of the pinning angles is most likely a formidable task, and the strong dispersion of the experimental data in the literature [23] could indicate that difficulty. In addition, the ignorance of a precise value of the diffusion constant prevents us from converting our diffusion length into a precise physical velocity. Second, we have observed in our numerics that, for a different set of parameters, at a reduced velocity, the minimum of the undercooling becomes less pronounced, and it is difficult to decide whether the curve would still exhibit a minimum at smaller V; if it does the minimum moves very close to the critical point where parity breaking occurs. We cannot state, at present, whether the existence of a minimum undercooling for *tilted* solutions is a generic feature or not. We would like in addition to point out that there has been until now neither a proof that the pattern should operate at the minimum undercooling nor that the average undercooling is an appropriate quantity for the selection mechanism.

Finally we want to say a few words on the region of the eutectic phase diagram that we have explored. The above results are computed for hypereutectics compositions ($c_\infty > c_e$). One might think that the deviation from the eutectic composition plays the role of some driving force [24,12]. We are then led to ask whether the above results would be markedly modified for eutectic or hypoeutectic compositions. We have made a systematic study of parity-broken states by varying $u_\infty \equiv (c_\infty - c_e)/\Delta c$ from -0.14 to 0.1. The main conclusion that we can draw is that the overall picture, presented above, remains qualitatively unaltered. We will not, therefore, linger on details and simply show how the velocity, for a fixed tilt angle, changes with u_∞ (Fig. 8) and two front profiles for a positive and a negative value of u_∞, namely $u_\infty = -0.1$ and 0.1 (Fig. 9). One sees in Fig. 8 that V increases by decreasing u_∞. This can be understood by first noticing that, due to global mass conservation, the volume fraction of the β phase decreases by decreasing u_∞ (see Fig. 9). This means that its stiffness (which is measured on the scale of its width) becomes more and more pronounced. As a consequence the threshold for parity breaking is increased.

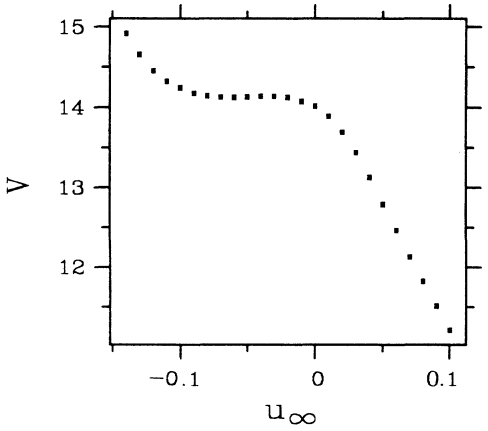

FIG. 8. The velocity for a fixed tilt angle ($\phi = 28.6°$) as a function of u_∞. Other parameters as in Fig. 4.

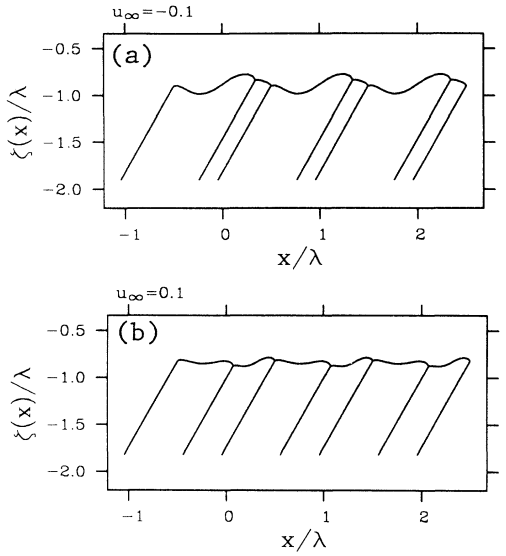

FIG. 9. Tilted front profiles computed with two different values of u_∞ explored in the numerics. (a) $u_\infty = -0.1$, (b) $u_\infty = 0.1$. Parameters and tilt angle as in Fig. 8.

IV. SIMILARITY EQUATION

One interesting feature of eutectic growth lies in the smallness of the Péclet number, defined here as $P = \lambda/l$. In standard experiments $P \sim 10^{-2}$. This fact allows, by introduction of appropriate dimensionless quantities, to scale this number out from the governing equations. As a consequence we can write down some general similarity laws of the pattern. In previous work we have shown [10], by taking as a staring point the integral equation for symmetric lamellae, that the full boundary integral equation reduces, in the small Péclet number limit, to a similarity equation containing only two dimensionless parameters. These parameters can be taken as $\sigma = d_0^\alpha l/\lambda^2$ and $\chi = l/l_T^\alpha$. The small Péclet number limit is not uniform and care should be taken when performing it. More recently [11] we have given a rigorous derivation of our similarity equation and emphasized the main subtleties. Our previous derivation [11] critically depended, however, on the reflection symmetry about the growth axis. Without this symmetry, a certain integral would have diverged in the small Péclet number limit. This means that the extension of the derivation of the similarity equation to the present case should involve additional difficulties. It can be shown, however, that this problem can be resolved. To attempt to give here an account of

the mathematical sophistication that is involved in the derivation of the similarity equation would be tangential to our present purposes, so we shall give the result and simply point out some of the difficulties. The extensive derivation is planned to be published elsewhere [13].

Let us first rewrite Eq. (2.12) explicitly by introducing λ as a length scale instead of l. We are then to understand that we should multiply all the lengths in Eq. (2.12) by P. By making explicit the normal derivative, Eq. (2.12) takes the form

$$\frac{\tilde{u}(x)}{2}=\frac{u_\infty}{P}+\frac{1}{2\pi}\int_{-\infty}^{\infty}dx' e^{-P[\Delta\zeta+\Delta x\tan(\phi)]}[1-\zeta_{x'}\tan(\phi)]\{2H(x')+P[1-2k(x')]\tilde{u}(x')\}K_0\left[P\frac{\rho}{\cos(\phi)}\right]$$
$$+\frac{P}{2\pi}\int_{-\infty}^{\infty}dx' e^{-P[\Delta\zeta+\Delta x\tan(\phi)]}\frac{\Delta\zeta-\Delta x\zeta_{x'}}{\rho\cos(\phi)}\tilde{u}(x')K_1\left[P\frac{\rho}{\cos(\phi)}\right], \tag{4.1}$$

where $\tilde{u}(x)$ is defined as

$$u=-P\epsilon(x)[\chi\zeta(x)+\psi(x)\sigma\kappa(x)]\equiv P\tilde{u}(x)\ , \tag{4.2}$$

with

$$\epsilon(x)=\begin{cases}1, & \alpha \text{ phase}\\ -l_T^\alpha/l_T^\beta, & \beta \text{ phase}\ ,\end{cases} \tag{4.3}$$

$$\psi(x)=\begin{cases}1, & \alpha \text{ phase}\\ l_T^\beta d_0^\beta/l_T^\alpha d_0^\alpha, & \beta \text{ phase}\ ,\end{cases} \tag{4.4}$$

$$k(x)=\begin{cases}k_\alpha, & \alpha \text{ phase}\\ k_\beta, & \beta \text{ phase}\ ,\end{cases} \tag{4.5}$$

$$H(x)=\begin{cases}\delta, & \alpha \text{ phase}\\ \delta-1, & \beta \text{ phase}\ ,\end{cases} \tag{4.6}$$

all of which are piecewise constant functions. K_1 is the modified Bessel function of order one. Note that in Eq. (4.1) u_∞, which appears in Eq. (2.12), has been moved in front of the integral by making use of the sum rule

$$\int_{\Gamma_{sl}}d\Gamma' h(\mathbf{r},\mathbf{r}')=-1\ , \tag{4.7}$$

which is derived in the Appendix.

Let us point out very briefly that the limit $P\to 0$ of Eq. (4.1) is not trivial. First, on naively taking the limit $P\to 0$ we are faced with two divergences, one coming from u_∞/P (the first term on the right-hand side) and the second being the logarithmic singularity originating from the small argument expansion of K_0. In our previous work [10,11] we have shown how to circumvent the second divergence. This has consisted of adding to that divergence and subtracting from it an integral that we could evaluate exactly. The subtraction has served to cancel the divergence. In evaluating the added part, however, we ended up with a right-hand side of the form $(u_\infty+\delta+\eta-1)/P$, where η is the volume fraction of the α phase, apparently diverging as $1/P$. However by realizing that the numerator is nothing but the diffusion layer that forms ahead of the front, we could expect it to be of the order of P. This has been shown by making use of the mass conservation law on the global scale [10,11]. The question still arose of whether we were allowed, after extracting those divergences, to simply take the limits $P\to 0$ of each integrand. To do so legitimately the integrals should converge uniformly as P is sent to zero. We have discussed that issue recently [11]. For the K_0 term in Eq. (4.1) the analysis can follow, basically, step by step the one presented for axisymmetric growth [11]. For the K_1 term, however, a central point of the derivation was based on the symmetry of the pattern about the growth axis. As mentioned above the problem can be resolved for nonaxisymmetric pattern, but this involves some other mathematical details that we will avoid here. The similarity equation for the present case reads [13]

$$-\frac{\epsilon(x)}{2}[\chi\zeta(x)+\psi(x)\sigma\kappa(x)]=-\int_0^1 dx'\frac{\epsilon(x')}{2}[\chi\zeta(x')+\psi(x')\sigma\kappa(x')]-\int_0^1 dx'\Delta\zeta[1-\zeta_{x'}\tan(\phi)]H(x')$$
$$+\frac{1}{\pi}\int_{-\infty}^{\infty}dx'[1-\zeta_{x'}\tan(\phi)]H(x')\ln\frac{|\Delta x|}{\rho}+\sum_{n=1}^{\infty}\frac{\sin n\pi x_e}{(n\pi)^2}\cos 2n\pi\left[x-\frac{x_e}{2}\right]$$
$$+\frac{1}{\pi}\tan(\phi)\int_0^1 dx'\zeta_{x'}H(x')\ln(2|\sin\pi\Delta x|)$$
$$-\frac{1}{2\pi}\fint_{-\infty}^{\infty}dx'\frac{\Delta\zeta-\Delta x\zeta_{x'}}{\rho^2}\epsilon(x')[\chi\zeta(x')+\psi(x')\sigma\kappa(x')]\ . \tag{4.8}$$

We have defined here $\fint_{-\infty}^{\infty} dx' \ldots = \lim_{R\to\infty} \int_{-R}^{R} dx' \ldots$. In the limit $\phi \to 0$ we recover the similarity equation derived for symmetric growth. The first consequence of the similarity equation is that the pattern properties depend on only two dimensionless *dynamical* quantities σ and χ—all other parameters are material constants. In particular, the pattern is self-similar under a stretching (shrinkage) of λ and (G, V) by a positive factor α and α^{-2}, respectively. We have discussed previously the similarity of the pattern. Here we will consider only one aspect related to the scaling of the tilt angle. From Eq. (4.1) we see that the tilt angle $\phi = \phi(\sigma, \chi)$. We can then test our results by integrating the original equation (2.12). Figure 10 shows the results. The triangles represent the tilt angle for a fixed σ value and a fixed thermal gradient (or thermal length). This is the usual experimental situation [4]. It is clear that the tilt angle is approximately constant for large enough velocities (more precisely for l_T/l of a few unities; the physical units in that figure are recalled in the caption), which is in agreement with experimental observations [4]. For smaller V we obtain a drastic variation of the tilt angle with V. Although, as mentioned in Sec. IV, ignorance of precise values of some physical parameters prevents us from a complete numerical comparison with experiments; we believe that the range of V values where ϕ significantly decreases is safely in the accessible experimental range. The squares in Fig. 10 represent the tilt angle for fixed σ and χ. Fixing the value of χ is not the usual experimental procedure, but its realization poses no specific challenge. It is clear in Fig. 10 that the tilt angle ϕ is approximately constant in a wide range of the growth velocity. We hope that this simple prediction constitutes a call for an experimental check.

The reason why the tilt angle ϕ decreases with V when σ and l_T (rather than χ) are fixed is easy to understand. Indeed, due to the similarity properties a decrease in V implies a variation of the parameter χ which is equivalent to an increase by the same amount in the thermal gradient. When V has appreciably decreased, the (virtual) increase of the thermal gradient becomes so strong that it acts against the development of parity-broken states, which are always accompanied by a distortion of the interface pushing the solid (liquid) towards the hot (cold) contact. In other words the thermal gradient suppresses the tendency of tilting. As a result the tilt angle should decrease. This is expressed by the triangles in Fig. 10. Other consequences of similarity in tilted growth are planned to be discussed elsewhere [13].

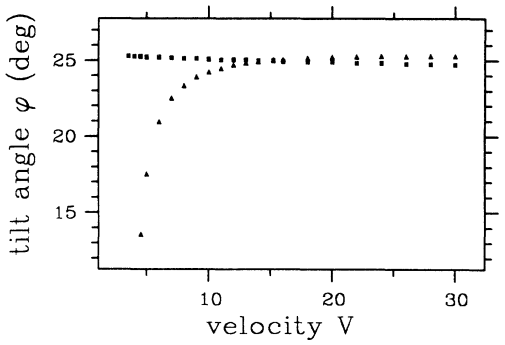

FIG. 10. The tilt angle ϕ as a function of the velocity. The material parameters are the same as in Fig. 4. The data represented by squares correspond to $l_T^{\alpha} = l_T^{\beta} = 1.0$. V and λ were varied simultaneously such that $\lambda^2 V = \text{const}$ (and hence $\sigma = \text{const}$, because $d_0^{\alpha/\beta}$ were kept fixed). In this way, λ was varied between 0.0074 and 0.025. To obtain the data drawn as triangles, V and λ were chosen as before, but $l_T = l_T^{\alpha} = l_T^{\beta}$ was varied as well to keep l/l_T constant.

V. DISCUSSION OF THE RESULTS AND SOME IMPLICATIONS

Here we have considered a situation where parity-broken states fill the entire front. However in different systems [4,6,7] parity-broken states appear as localized inclusions. These observations have led to the denomination solitary modes. An important question thus arises. Does parity breaking necessarily imply solitary or localized states? This is, in our opinion, far from true. In particular we have seen here that the birfurcation of the symmetric state into the asymmetric one is forward. This bifurcation occurs if one approximately doubles the wavelength of the symmetric state, which is assumed—as seems often to be the case in experiments—to operate at the minimum undercooling. How could one double the wavelength of the symmetric state? An answer to this question is provided by first noticing that the wavelength of the pattern λ scales with the growth velocity V as $\lambda \sim V^{-1/2}$. Hence, if we suddenly multiply V by a factor of 4 (or so), we will temporarily force the whole front to have a wavelength twice as large as the one it would have selected if that velocity were adiabatically achieved. Our results then tell us that the symmetric state should undergo a parity-breaking transition as a whole.

Previous experiments [4] observed only localized inclusions of tilted lamellae after a small velocity jump. This is, in view of the results that have emerged here, not surprising as a small velocity jump can, at best, cause only local wavelength fluctuations, most likely close to grain boundaries. How the localized asymmetric domain then evolves with time, or more precisely, what is the driving force that leads to the spreading or collapse of that domain is a question that is beyond the scope of the present study. Our main message is that for the asymmetric lamellae to fill the front as a whole one should double the wavelength of the symmetric state. An implication of our study is that the soliton notion should depend on the experimental protocol.

Had the bifurcation been subcritical, then we would have legitimately expected, *a priori,* the soliton notion to be related to an intrinsic feature of the system in the metastability domain. However, as parity breaking occurs as an interplay between two competing lengths (the diffusion and capillary length) which have two very different scales, one expects any possible metastability domain to be extremely narrow, beyond experimental resolution.

Finally we would like to make some remarks related to the stability of the upper branches for symmetric patterns

(Fig. 7). We have seen that parity-broken states emerge close to the fold of the lower pair of branches associated with the symmetric state. The picture in Fig. 7 conveys the strong impression that close to the upper fold another branch (with a higher undercooling) should exist. We have not yet attempted to investigate this question and hope to deal with it in the near future. Let us assume, as we suspect, that indeed that branch exists. The point where it bifurcates should, therefore, correspond to a loss of stability of the symmetric state. This would imply that the lower branch of the upper pair for symmetric states should be—at least close enough to the critical point for the emergence of the (hypothetical) branch for tilted solutions—stable. This is a purely bifurcation-based argument. If our speculation is confirmed then the lower branch of the upper pair for symmetric solutions should be most likely metastable (when this notion has a meaning) rather than unstable as we could expect by looking to the front profile [11]. It is imperative to perform a full linear-stability analysis, not only to settle the above questions, but also to draw a general picture for all types of instabilities of both the symmetric and asymmetric states.

VI. CONCLUSION

Here we sum up the main results that follow from the present analysis.

(i) We have shown that the fully isotropic model of directional growth of lamellar eutectics supports solutions with a broken parity. These solutions appear, for the range of parameters explored so far as a forward bifurcation of the symmetric state. Bifurcations are, generically, accompanied by the loss of some symmetry. In the present case it is parity breaking that accompanies the bifurcation. In order to destabilize the symmetric state, and provided that it operates at the minimum undercooling, its wavelength should be (approximately) doubled.

(ii) The fact that the wavelength of the asymmetric state is about twice as large as that of the symmetric one combined with the approximate scaling law $\lambda \sim V^{-1/2}$ tells us that a sudden jump of the growth velocity by a factor of 4 (or so) should lead to parity breaking of, virtually, the whole front. If such is the case then the denomination soliton will not be legitimate.

(iii) We have demonstrated that tilted solutions exist for off-eutectic as well as for eutectic compositions. Until now experimental investigations [4] considered only the situation with hypereutectic compositions. We hope that this work will call for new experiments with the aim to investigate the possibility of tilted growth at eutectic and hypoeutectic compositions.

(iv) Finally, because of the smallness of the Péclet number in standard experiments, we have been able to derive a general similarity equation. The limit of small Péclet numbers is not uniform. We have mentioned the main difficulties encountered when performing this limit. It was not appropriate in our case to go through the (lengthy) mathematics of the derivation of the similarity equation, which otherwise would have been done at the expense of other results whose presentation is closer to the spirit of this article. We have confirmed the similarity consequences by numerically integrating the original equations. We have shown that, in particular, the tilt angle ϕ depends on the combinations $\lambda^2 V$ only for large enough growth velocities but should drastically depend on the combination G/V (G being the thermal gradient) also, for smaller velocities. We hope that these predictions will incite new experiments.

ACKNOWLEDGMENTS

One of us (C.M.) acknowledges financial support from "Centre National d'Etudes Spatiales."

APPENDIX: THE SUM RULE IN TILTED GROWTH

There have been various derivations of sum rules for the Green's functions used in the description of dendritic growth or directional solidification [17,25]. We found that the previous approach using the asymptotic expansion of Bessel functions to reduce the sum rule of a stationary system to integrals of Gaussians [25] does not work, if the motion of the interface is not parallel to the z axis. It should, of course, be possible to specialize the general sum rule for the time-dependent case [17] to the present situation. We prefer, however, to give a direct derivation for the current stationary system on the basis of the properties of the modified Bessel functions. This allows us to more clearly see that in the stationary case there is no need to move most of the integration contour to infinity.

We start from the fact that $u = u_0 = \text{const}$ solves the diffusion equation and hence also the integral equations (2.8) for any *closed* contour Γ. This entails

$$\int_{\Gamma} d\Gamma' h(\mathbf{r},\mathbf{r}') = 0 \ . \tag{A1}$$

For our purposes, the most useful contour is obtained by adding to Γ_{sl} a piece Γ_Z running from $x' = \infty$ to $x' = -\infty$ at a value $z' = Z > 0$ and joining it to Γ_{sl} at the infinitely far endpoints by pieces $\Gamma_{\parallel 1}$ and $\Gamma_{\parallel 2}$ which are parallel to the z axis (see Fig. 11). Written out explicitly, $h(\mathbf{r},\mathbf{r}')$ reads

$$\begin{aligned} h(\mathbf{r},\mathbf{r}') = \frac{1}{2\pi l} e^{-(z-z')/l - \tan(\phi)(x-x')/l} \\ \times \left[-[n_z' + \tan(\phi) n_x'] K_0 \left(\frac{|\mathbf{r}-\mathbf{r}'|}{\cos(\phi) l} \right) \right. \\ \left. - \frac{\mathbf{n}'(\mathbf{r}'-\mathbf{r})}{\cos(\phi)|\mathbf{r}-\mathbf{r}'|} K_1 \left(\frac{|\mathbf{r}-\mathbf{r}'|}{\cos(\phi) l} \right) \right] \\ - \tfrac{1}{2} \delta(\mathbf{r}-\mathbf{r}') \ . \end{aligned} \tag{A2}$$

We require that $\mathbf{r}\ [=(x,z)]$ does not lie on Γ_Z, i.e., $z \neq Z$, so we can omit the δ-function term in the integral on contour Γ_Z. Introducing new variables $\Delta z = (z'-z)/l = (Z-z)/l$ and $y = (x'-x)/l$, we obtain for that integral

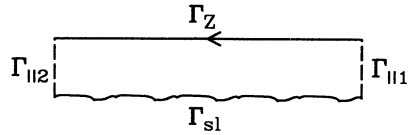

FIG. 11. Integration contour used in the derivation of the sum rule.

$$\int_{\Gamma_Z} d\Gamma' h(\mathbf{r},\mathbf{r}') = \frac{1}{2\pi} e^{\Delta z} \int_{-\infty}^{\infty} dy\, e^{\tan(\phi) y} \left[K_0 \left[\frac{\sqrt{y^2+\Delta z^2}}{\cos(\phi)} \right] + \frac{\Delta z}{\cos(\phi)\sqrt{y^2+\Delta z^2}} K_1 \left[\frac{\sqrt{y^2+\Delta z^2}}{\cos(\phi)} \right] \right] , \tag{A3}$$

where for Γ_Z, $d\Gamma' = -l\, dy$, $n_z' = -1$, and $n_x' = 0$. We call the first integral on the right-hand side of (A3) I_a, the second I_b. Both integrals can be evaluated exactly with the help of the following [26]:

$$\int_0^{\infty} dx\, K_\nu(\alpha\sqrt{x^2+z^2}) \frac{x^{2\mu+1}}{\sqrt{(x^2+z^2)^\nu}} = \frac{2^\mu \Gamma(\mu+1)}{\alpha^{\mu+1}|z|^{\nu-\mu-1}} K_{\nu-\mu-1}(\alpha|z|) , \tag{A4}$$

which holds for $\alpha > 0$, $\mathcal{R}(\mu) > -1$ and is written here for real z. From this formula, we obtain a series expansion for the integrals in (A3):

$$\begin{aligned} \int_{-\infty}^{\infty} dx\, e^{bx} K_\nu(\alpha\sqrt{x^2+z^2}) \frac{1}{\sqrt{(x^2+z^2)^\nu}} &= 2\int_0^{\infty} dx\, \cosh(bx) K_\nu(\alpha\sqrt{x^2+z^2}) \frac{1}{\sqrt{(x^2+z^2)^\nu}} \\ &= 2\sum_{n=0}^{\infty} \frac{b^{2n}}{(2n)!} \frac{2^{n-1/2}\Gamma(n+\frac{1}{2})}{\alpha^{n+1/2}|z|^{\nu-n-1/2}} K_{\nu-n-1/2}(\alpha|z|) , \end{aligned} \tag{A5}$$

where we have set $\mu = n - \frac{1}{2}$ to generate the series expansion of $\cosh bx$. The right-hand side of this equation can be simplified via the recursion relation [26]

$$\left[\frac{d}{z\, dz} \right]^m [z^\nu K_\nu(z)] = (-1)^m z^{\nu-m} K_{\nu-m}(z) , \tag{A6}$$

which leads to ($\tilde{z} = |z|$)

$$\begin{aligned} K_{\nu-n-1/2}(\alpha\tilde{z}) = (-1)^n (\alpha\tilde{z})^{n-\nu+1/2} &\left[\frac{d}{\alpha^2 \tilde{z}\, d\tilde{z}} \right]^n \\ &\times [(\alpha\tilde{z})^{\nu-1/2} K_{\nu-1/2}(\alpha\tilde{z})] . \end{aligned} \tag{A7}$$

Noting that

$$2^{n+1/2}\Gamma(n+\tfrac{1}{2})/(2n)! = \sqrt{2\pi}/(2^n n!) ,$$

we can write the right-hand side of (A5) as

$$\frac{\sqrt{2\pi}}{(\alpha\tilde{z}^2)^\nu} \tilde{z} \exp\left[-b^2 \tilde{z}'^2 \left[\frac{d}{2\alpha\tilde{z}\, d\alpha\tilde{z}} \right] \right] \times [(\alpha\tilde{z})^{\nu-1/2} K_{\nu-1/2}(\alpha\tilde{z})] \Big|_{\tilde{z}'=\tilde{z}} ,$$

where the introduction of $\tilde{z}'$ was necessary to avoid the differential operator acting on its prefactors containing $\tilde{z}$. Otherwise one would have had to write an infinite sum instead of the compact representation by the exponential of a differential operator. By substitution of variables, $w = (\alpha\tilde{z})^2$, the exponential operator can be reduced to a simple translation operator, whose action is easily evaluated:

$$\exp\left[-b^2\tilde{z}'^2 \frac{d}{dw} \right] f(w) = f(w - b^2\tilde{z}'^2) . \tag{A8}$$

This leads to the final result for the integral (A5)

$$\begin{aligned} \int_{-\infty}^{\infty} dx\, e^{bx} K_\nu(\alpha\sqrt{x^2+z^2}) \frac{1}{\sqrt{(x^2+z^2)^\nu}} &= \frac{\sqrt{2\pi}}{(\alpha z^2)^\nu} |z| (\sqrt{\alpha^2-b^2}|z|)^{\nu-1/2} \\ &\times K_{\nu-1/2}(\sqrt{\alpha^2-b^2}|z|) , \end{aligned} \tag{A9}$$

where a sufficient (and for some values of ν necessary) condition for convergence is that $\alpha > \mathcal{R}(b)$. In order to evaluate I_a and I_b, we need (A9) for $\nu = 0$ and $\nu = 1$. But then the formula generates half-integer order Bessel functions which are elementary. In particular,

$$K_{\pm 1/2}(z) = \sqrt{(\pi/2z)}\, e^{-z} , \tag{A10}$$

which leads to

$$\int_{-\infty}^{\infty} dx\, e^{bx} K_0(\alpha\sqrt{x^2+z^2}) = \frac{\pi}{\sqrt{\alpha^2-b^2}} e^{-\sqrt{\alpha^2-b^2}|z|} , \tag{A11}$$

$$\int_{-\infty}^{\infty} dx\, e^{bx} \frac{K_1(\alpha\sqrt{x^2+z^2})}{\sqrt{x^2+z^2}} = \frac{\pi}{\alpha|z|} e^{-\sqrt{\alpha^2-b^2}|z|} . \quad \text{(A12)}$$

In I_a and I_b, $\alpha=1/\cos(\phi)$ and $b=\tan(\phi)$, which gives $\sqrt{\alpha^2-b^2}=1$. Therefore, we obtain

$$I_a = \pi e^{-|\Delta z|} , \quad \text{(A13)}$$

$$I_b = \pm\pi e^{-|\Delta z|} , \quad \text{(A14)}$$

where the sign of I_b is equal to the sign of Δz. Inserting these results back into (A3), we finally arrive at [27,28]

$$\int_{\Gamma_Z} d\Gamma' h(\mathbf{r},\mathbf{r}') = \begin{cases} 1 & \text{if } Z > z \\ 0 & \text{if } Z < z \end{cases} . \quad \text{(A15)}$$

Since the used form of the integral equation is valid for a normal vector pointing *into* the domain encircled by Γ, the integration contour should be closed *above* Γ_{sl}, so we have $Z > z$. Because the integral on the complete contour Γ is zero and there is no contribution by the contours $\Gamma_{\parallel 1}$ and $\Gamma_{\parallel 2}$ (which have finite length), due to the exponential decay of K_0 and K_1 for $x' \to \pm\infty$, we end up with

$$\int_{\Gamma_{sl}} d\Gamma' h(\mathbf{r},\mathbf{r}') = -1 . \quad \text{(A16)}$$

[1] J. D. Hunt and K. A. Jackson, Trans. Metall. Soc. AIME **236**, 843 (1966).

[2] V. Seetharaman and R. Trivedi, Metall. Trans. **19A**, 2955 (1988).

[3] W. Kurz and D. J. Fisher, *Fundamentals of Solidification* (Trans. Tech., Aedermans dorf, 1984).

[4] G. Faivre, S. de Cheveigné, C. Guthmann, and P. Kurowski, Europhys. Lett. **9**, 779 (1989).

[5] R. Racek, Thèse d'Université, 1973; see also H. E. Cline, Mater. Sci. Eng. **65**, 93 (1984).

[6] A. J. Simon, J. Bechhofer, and A. Libchaber, Phys. Rev. Lett. **61**, 2574 (1988).

[7] M. Rabaud, S. Michalland, and Y. Couder, Phys. Rev. Lett. **64**, 184 (1990).

[8] P. Coullet, R. Goldstein, and G. H. Gunaratne, Phys. Rev. Lett. **63**, 1954 (1989).

[9] K. Kassner and C. Misbah, Phys. Rev. Lett. **65**, 1458 (1990); **66**, 522(E) (1991). For other interesting related works see H. Levine, W. J. Rappel, and H. Riecke, Phys. Rev. A **43**, 1122 (1991); H. Levine and W. J. Rappel, *ibid.* **42**, 7475 (1990); S. Fauve, S. Douady, and O. Thual, Phys. Rev. Lett. **65**, 385 (1990).

[10] K. Kassner and C. Misbah, Phys. Rev. Lett. **66**, 445 (1991).

[11] K. Kassner and C. Misbah, preceding paper, Phys. Rev. A **44**, 6513 (1991).

[12] A. Karma, Phys. Rev. Lett. **59**, 71 (1987).

[13] K. Kassner and C. Misbah (unpublished).

[14] Note that Eqs. (2.3) are in fact a simpification of the exact mass conservation equations for a nondilute system. Indeed, the terms in the square brackets must be understood as $(c_l - c_{si})$, $i=\alpha,\beta$. Thermodynamic equilibrium on the front imposes that (see Ref. [15]) $(c_{si}-c_i) = k(c_l-c_e)+d_0^c\kappa$, where κ is the front curvature. The capillary length d_0^c, which vanishes for dilute alloys, turns out to be negligible for eutectics with small temperature gaps $(m_i\Delta c_i)$. This is the case for the $CBr_4-C_2Cl_6$ eutectic in which we are interested here. We should, however, keep in mind that there are some eutectics for which d_0^c is not small, especially due to a large temperature gap (e.g., Pb−Sn).

[15] C. Misbah, J. Phys. (Paris) **47**, 1077 (1986).

[16] We should mention that strictly speaking the latent heats that enter the definition of the capillary lengths d_0^i are not exactly those of the α-liquid and β-liquid transitions, but effective quantities. The derivation given in Ref. [15] for a quasiazeotrope may serve as a guide for a check of this remark. We see there that only because the concentrations of the solid and liquid phases are equal at the azeotropic point (which is not the case for eutectics), the effective heat of transition reduces to the latent heat.

[17] B. Caroli, C. Caroli, B. Roulet, and J. S. Langer, Phys. Rev. A **33**, 442 (1986).

[18] J. W. McLean and P. G. Saffman, J. Fluid Mech. **122**, 455 (1981).

[19] L. H. Ungar and R. A. Brown, Phys. Rev. B **29**, 1367 (1984); **30**, 3993 (1984); **31**, 5923 (1985); **31**, 5931 (1985).

[20] W. W. Mullins and R. F. Sekerka, J. Appl. Phys. **35D**, 444 (1964).

[21] K. A. Jackson and J. D. Hunt, Trans. Metal Soc. AIME **236**, 1129 (1966).

[22] To our knowledge, this argument is known as the Cahn argument as reported by Jackson and Hunt (Ref. [21]).

[23] W. K. Kaukler and J. W. Rutter, in *In Situ Composites IV*, edited by F. D. Lemkey, H. E. Cline, and M. McLean (Elsevier, New York, 1982).

[24] V. Datye and J. S. Langer, Phys. Rev. B **24**, 4155 (1981).

[25] Y. Saito, G. Goldbeck-Wood, and H. Müller-Krumbhaar, Phys. Rev. A **38**, 2148 (1988).

[26] I. S. Gradshteyn and I. M. Ryzhik, *Table of Integrals, Series, and Products* (Academic, Orlando, 1980), Nos. 6.596,3 and 8.468,14.

[27] C. A. Brebbia, *The Boundary Element Method for Engineers* (Penetech, London, 1978).

[28] *Handbook of Mathematical Functions*, edited by M. Abramowitz and I. A. Stegun (Dover, New York, 1972).